



## A probabilistic approach to online classification of bicycle crashes

Jan Schnee<sup>a,\*</sup>, Jürgen Stegmaier<sup>a</sup>, Pu Li<sup>b</sup>

<sup>a</sup> Robert Bosch GmbH, 70839 Gerlingen-Schillerhoehe, Germany

<sup>b</sup> Institute for Automation and System Engineering, Ilmenau University of Technology, 98693 Ilmenau, Germany



### ARTICLE INFO

#### Keywords:

Bicycle crash classification  
Crash detection  
Logit model  
ANOVA  
IMU  
Probabilistic modeling

### ABSTRACT

When a bicycle crash takes place, it is paramount for an emergency center to recognize the physical state of the cyclist as early as possible. However, an injured bicyclist may be incapable of making a phone call to the emergency center. In this study, we propose an online approach to classify bicycle crashes based on signals from an onboard inertial measurement unit (IMU), which can be used as a trigger function for an automatic emergency system. For this purpose, we define several bicycle crash features according to the kinematic properties of bicycle accidents. The input signals (variables) influencing the individual crash features are determined by the ANOVA method (analysis of variance). With the determined input signals, probabilistic models for each crash feature are trained on the base of logit models and 20,000 km naturalistic driving data including 20 real crashes. In addition, further crash and corner case data has been collected for the model training. A decision tree describing all probabilistic crash features is used to classify different kinematic events and crash scenarios. A series of driving tests with a crash-dummy and a crash-car are performed to verify the proposed crash classification approach, showing a sensitivity of 96.8%, a specificity of 99.6% and an accuracy of 99.5% of the trained model.

### 1. Introduction

Electrically power assisted cycles (EPACs) show a tremendous growth in sales figures (Statista, 2019). Schepers et al. (2014) justified this trend in the last decade because of the health and environmental benefits introduced by EPACs. The current pandemic situation leads to a further boost of that boom (Roberson, 2020) due to social distancing rules and the limited amount of possible activities during the lock-down.

However, this increasing group of vulnerable road users also leads to growing accident numbers: In Germany in 2019, 87,253 bicycle accidents (11% from EPACs) have been reported officially in which 15,176 cyclists (16% from EPAC riders) were seriously injured and 445 cyclists (including 118 EPAC riders) died (Statistisches Bundesamt, 2020). Further studies revealed that 70% of bicycle accidents remain officially unreported (Bundesamt fuer Strassenwesen, 2016) and up to 80% are single-vehicle accidents (Hagemeister et al., 2015). These studies reinforce an urgent need for countermeasures (Zhang and Jiang, 2017) to improve the safety of cyclists.

Chavis et al. (2018) analyzed the conditions and effects for the root causes of bicycle crash scenarios based on different databases. One major problem of these databases is the major underreporting (Juhra et al., 2012) of bicycle crashes caused by not officially reported single-

vehicle accidents.

Based on such accident researches, studies were made to improve the cyclists' safety, by focusing on the infrastructure used by the bicyclists (DiGioia et al., 2017; Pucher and Buehler, 2016) and on the impact of the safety gear (Olivier and Creighton, 2016). In addition, bicycle assistant safety systems were intensively studied (Smaldone et al., 2010; Chen et al., 2019; Maier et al., 2015). In 2018, Bosch introduced the first commercial anti-lock braking system for EPACs (Bosch eBike, 2018). Furthermore, Rajamani et al. (2018) developed a sonar-based collision avoidance system for preventing car-bicycle accidents.

To date, there have been only limited studies available on bicycle crash detection. Candefjord et al. (2014) investigated a crash detection approach for bicycles based on the IMU data from smartphones. Gelmini et al. (2019) analyzed a crash detection approach for two-wheeled vehicles. However, the results of these studies need to be validated by a great variety of bicycling data. In addition, manufacturers of bicycle equipment introduced smart helmets (Specialized; Tocsen) and bike onboard computers with crash detection systems (Garmin). In Usami et al. (2018) and Gu et al. (2017) dangerous cycling behaviors were analyzed and the presented methods aimed to predict and detect these situations based on smartphone sensor data for accident prevention. Automatic detection or classification of bicycle accidents are not in the

\* Corresponding author.

E-mail address: [jan.schnee@de.bosch.com](mailto:jan.schnee@de.bosch.com) (J. Schnee).

focus of both studies. A recent study on a bicycle accident detection was presented by Tabei et al. (2021). 3-axis acceleration, gyroscope and magnetic field data were used by the principal component analysis for feature reduction and a support vector machine for the crash event detection. The set up dataset was recorded with one bicycle only and had the focus on single vehicle fall accidents. Neither collision scenarios nor corner cases regarding the mountain bike use case such as drops or jumps and further daily riding data were considered. To the best of our knowledge, an automatic classification of bicycle crash events regarding the accident sequence has not been investigated yet.

On the other hand, in automotive or motorbike applications, a variety of safety functions have been applied for crash detection (Bonyr et al., 2017). introduced an automatic crash detection for motorcycles based on IMUs placed on the rider and the motorbike itself. However, such a system is not suitable for the bicycle use case because of its complex sensor setup and the different vehicle dynamics.

In this paper, we propose an automatic classification approach for bicycle crashes which can be used as a real-time automatic emergency reporting system. Crash classes are categorized according to their kinematic trajectories and characteristics based on the measured data from an onboard IMU. We define bicycle specific kinematic crash features which are modeled with the logistic regression method and analyzed by further machine learning methods. The feature model is then trained based on a large database of cycling and crash data. Finally, the trained model is verified by a large validation dataset including an extensive crash test series. Besides the usage as a trigger function for an automatic emergency reporting system, our approach also allows automatic data acquisition of crash events for further accident studies.

The proposed approach and the results of the model training are presented in Section 2. Section 3 describes the data acquisition and the database utilized for training and validating the model. It is followed in Section 4 by the model validation results and the discussion. Section 5 summarizes the paper.

## 2. Methodology

The aim of this study is to develop an approach for classifying bicycle crashes according to the specific kinematic scenario of an accident. For this purpose, IMU data from a sensor mounted on the bicycle frame will be used as input. Fig. 1 shows the computational framework of the proposed approach.

At the beginning, the database presented in Section 3 is split into a

training and a validation dataset. The training dataset is processed by several computational steps which will be presented in detail in the following subsections. The validation data are necessary to verify the trained model (see Section 4.1 and 4.2) for ensuring an unbiased model evaluation.

### 2.1. Definition of bicycle crash features

In this study, the data used for crash classification are from an IMU mounted on the bicycle frame. German definitions for transport accidents classify separate crashes in transport according to the situation of conflict, which caused the incident ("accident-type", Ortlepp et al., 2016). Besides that, a further categorization is usually used regarding the "collision-type" (Statistisches Bundesamt, 2020). Using the onboard IMU data, these two types cannot be distinguished in effect, and thus further meta-information (e.g. the type and state of other participants involved) is required. However, the onboard IMU data provide the kinematic trajectory of the bicycle which can be utilized to detect specific features of an accident. Therefore, we define four typical bicycle crash features (see Table 1). This crash feature concept is similar to the model architecture presented by Parviaainen et al. (2014) for the motorbike use case.

The defined crash features shown in Table 1 enable the reconstruction of the kinematic states of a bicycle during normal riding scenarios as

**Table 1**  
Definition of bicycle crash features and polytomous states.

#	Name	Description	States
1	Ride (Rd)	riding state, right before accident	0: standing 1: starting/stopping 2: riding
2	Collision (C)	collision with a rigid obstacle or further party involved	0: no collision 1: soft collision 2: medium collision 3: strong collision
3	GroundHit (GH)	impact when a bicycle is tipping over	0: false, 1: true
4	TipOver (TO)	orientation of bicycle, bicycle rolled over	0: upright bicycle 1: TipOver (RollOver) 2: NoseOver

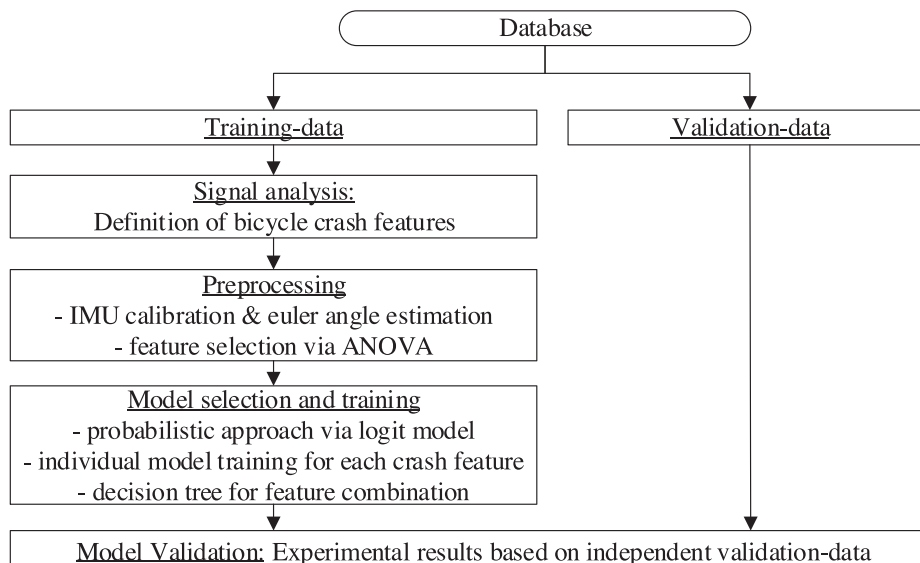


**Fig. 1.** Sequence overview of the used methods.

well as during accident situations. In addition, these features allow to distinguish crash events from bicycle specific corner cases like dropping the bike to one side, putting the bike horizontally into the trunk of the car or riding a wall ride in a bike park. Furthermore, the defined crash features are specific for the bicycle use case, i.e. they are clearly different from the automotive or motorbike use cases. By combining these four features and their corresponding states, the proposed approach is able to classify different kinematic scenarios. Detailed analysis of the feature combination and the crash classification method are presented in Section 2.4.

## 2.2. Preprocessing and data analysis

A 6DOF-IMU (i.e. 6 dimensions of freedom, 3 axis accelerometer and 3 axis gyroscope) mounted on the bicycle is used to collect the data in the sensor coordinate system. The sensor has a rigid link to the bicycle frame, but the location and orientation on the frame can be freely set up due to the rigid body characteristics of the bicycle frame. For estimating the orientation of the bicycle as well as determining the other crash features, the data are transformed into the vehicle frame coordinate system (Iso 8855:2011, 2011). The online auto-calibration scheme presented by Schnee et al. (2020) is implemented for this pre-processing step.

After the calibration, a sensor fusion method (Madgwick, 2010; Sabatini, 2006) is used for estimating the Euler angles (roll  $\phi$  and pitch  $\theta$ ) of the bicycle based on the accelerometer and gyroscope data. The dynamic bicycle orientation for the crash feature models is expressed as

$$\gamma = \sqrt{\phi^2 + \theta^2} \quad (1)$$

where  $\gamma$  is the combined orientation signal of the fused Euler angles  $\phi$  and  $\theta$ . In addition, the delayed bicycle orientation is calculated as follows:

$$\gamma_{acc} = \text{atan} \left( \frac{\sqrt{a_{Bf,Lp,x}^2 + a_{Bf,Lp,y}^2}}{|a_{Bf,Lp,z}|} \right) \quad (2)$$

where  $\gamma_{acc}$  depends on the low-pass (LP) filtered acceleration signals in the bicycle frame system  $Bf$  ( $a_{Bf,Lp,x}$ ,  $a_{Bf,Lp,y}$ ,  $a_{Bf,Lp,z}$ ). The delay of  $\gamma_{acc}$  represents a property required for the TipOver feature. For estimating the defined TipOver feature (see Table 1) an additional input variable is needed:

$$\psi = \frac{|\theta|}{|\phi|} \quad (3)$$

where  $\psi$  describes the relation between the Euler angles  $\theta$  and  $\phi$ .

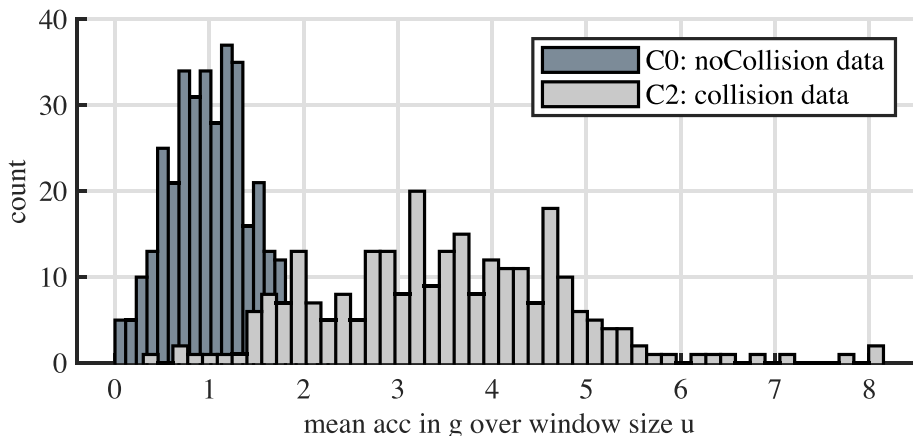


Fig. 2. Normally distributed pre-processed acceleration signals.

Our approach uses the measured speed of the system,  $v_{Bike}$ . If no speed measurement is available, the bike speed can be estimated by using an INS (inertial navigation system, Wu et al., 2005).

The modeling of the GroundHit and Collision features requires further independent pre-processed signals. For this purpose, we use the ANOVA (analysis of variance) approach (Dalgaard, 2008) to analyze different statistical properties (e.g. mean, standard deviation, variance, extrema, and integral Figo et al., 2010) over different window sizes of the IMU acceleration data. The ANOVA approach requires the pre-processed data to be normally distributed. We use the Anderson–Darling-Test (Scholz and Stephens, 1987) to verify this necessary condition. Fig. 2 shows an exemplary histogram to demonstrate the normal distribution for the mean acceleration over a defined window size  $u$ .

The result of the ANOVA analysis returns the specific energy as the optimal indicator among those from the investigated statistical approaches for classifying the Collision and GroundHit events as follows:

$$\Delta e_{xy,u}(i) = \left( \int_{i-u}^i a_{Bf,x}(k) dk \right)^2 + \left( \int_{i-u}^i a_{Bf,y}(k) dk \right)^2 \quad (4)$$

where  $\Delta e_{xy,u}$  represents the change of the mass specific kinetic energy. It describes an event in the xy-plane in the bicycle coordinate system (i.e. the bike frame (BF)) during the time window  $u$ , by the integration of the acceleration signals  $a_{Bf,x}$  and  $a_{Bf,y}$ . Since Collision and GroundHit events only take place in this plane, the effects in the vertical z-axis are traced back to the road surface or jumps of the bicycle system. In addition, the variance  $\sigma_{xy,u_{GH}}$  of the x- and y-acceleration signals over a time window  $u_{GH}$  provides further separation possibilities for GroundHit events.

The use of such energy approaches for impact analysis was introduced in automotive studies (Roelleke et al., 2001). According to our ANOVA results the window lengths  $u_C$  and  $u_{GH}$  are comparable to the results in the motorbike use case presented by Parviainen et al. (2014). In addition, it is shown that the window length  $u$  varies marginally between the two impact types (i.e. GroundHit and Collision).

## 2.3. Probabilistic model selection and training

Our aim for a bicycle crash classification is to estimate the type of the crash based on the kinematic trajectory of the bicycle. Besides the classification result, the model shall return a probability variable indicating the confidence regarding the current crash class estimation. Here, we use the logistic regression method to carry out this task.

In general, logistic regression fits a sigmoid function on some training data for determining probability estimates regarding a specific feature. The logit model we use in this study is defined as

$$p(\mathbf{X}) = \frac{1}{1 + e^{-\beta^T \mathbf{X}}} \quad (5)$$

where  $p(\mathbf{X})$  is the probability estimation of a binary feature, which can be interpreted as a confidence level.  $\beta$  is the corresponding hyper-parameter vector which is trained with input signals  $\mathbf{X}$  of the training data (Hastie et al., 2001, p.119ff).

The defined crash features (see Table 1) are built based on separate logit models. This manual technique of defining and handling each crash feature separately is used due to the small amount of available crash data (see Section 3), where the most influencing input variables can be determined manually for each crash feature, to reduce model overfitting. In Section 2.4, the approach for combining all logit models is presented. It is noted that the method of logistic regression is enhanced by the k-fold cross validation and lasso regularization for selecting optimal training data and to further reduce over-fitting onto the training data (Hastie et al., 2001, p.241ff; Algamal and Lee, 2015).

#### 2.4. Feature combination

After treating the crash features separately (see Section 2.5), a probabilistic decision tree is constructed to analyze the combining effect of the crash feature models, as shown in Fig. 3. These features are defined as stochastically independent probabilistic models, thus the shown decision tree presents all possible feature state combinations (except for C1 soft collisions, which cannot be distinguished during Rd1/Rd2 riding situations from general intense vibrations and therefore are consequently treated as C0 no collisions). This procedure leads to 60 kinematic output classes. We merge all 60 output scenarios into super-crash and sub-crash classes according to their similarities in the kinematic trajectories. If an event responds to the output with the crash class of '0', the corresponding kinematic scenario will not be defined as a bicycle accident.

We distinguish the combined scenarios with similar kinematic trajectories into 5 merged super-crash classes (i.e., 1X-5X), as shown in

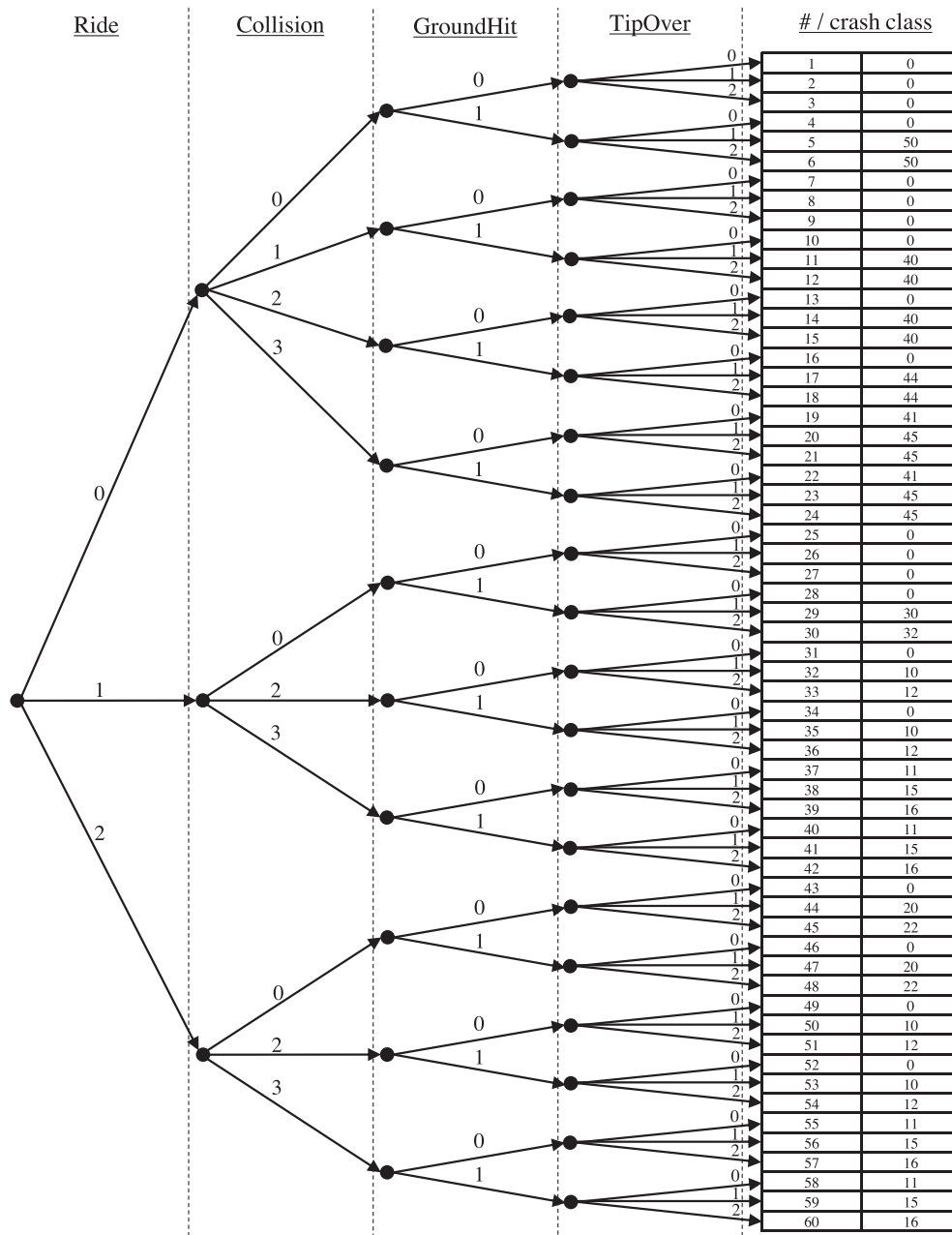


Fig. 3. Structure of decision tree for bicycle crash classification, including merged (super and sub) output crash classes.

**Table 2**

Definition of super crash classes.

super crash class	Description
1X	bicycle accident with some collision during riding
2X	bicycle accident with no collision during riding
3X	bicycle accident with no collision during low speed scenarios
4X	bicycle accident with some collision while standing
5X	bicycle accident with no collision while standing

**Table 2.**

In Fig. 3, the second digit of the numbers in the last column defines the sub-crash classes of the kinematic scenario and provides details about the collision type and TipOver state, i.e., whether a NoseOver, RollOver or no TipOver took place. For instance, a '1' indicates that the crash scenario does not show a TipOver (TO0) and a sub-crash class of '2' or '6' represents a NoseOver case (TO2). Further definitions for the sub-crash classes can be seen in Fig. 3.

For estimating the final output probability of each crash class of the decision tree, we use the multiplicative combination of all stochastically independent models as follows,

$$p_{0000}(P_{Rd0} \cap P_{C0} \cap P_{GH0} \cap P_{TO0}) = P_{Rd0} * P_{C0} * P_{GH0} * P_{TO0} \quad (6)$$

where  $p_{0000}$  is, as an example, the probability of the first output branch shown in Fig. 3. Its indices describe the corresponding kinematic bicycle scenario, i.e. all four crash features show the state '0' (i.e. Rd0, C0, GH0 and TO0). This case represents a standing bicycle which is upright and not experiencing any motion. The corresponding crash class is given in Fig. 3 as '0', since it represents a scenario with no crash event.  $P_{Rd0}, P_{C0}, P_{GH0}, P_{TO0}$  are the feature outputs which indicate the probability estimates for the specific feature states (see Section 2.5). All the other 59 scenarios and classification probabilities are estimated accordingly.

The overall crash probability  $p_c$  is defined as the sum of the output probabilities of all actual accident scenarios (crash class  $\neq$  '0').

## 2.5. Modeling of crash features

In this section, the model training of the individual crash features is presented based on the selected training data (see Section 3), which is implemented in MATLAB.

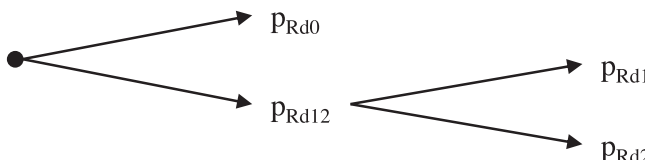
### 2.5.1. Ride feature

The ride feature indicates the state of driving in three states (see Table 1). The labeled Rd-data are processed in two binary stages, where each stage represents a separate logit model. The corresponding computational architecture is shown in Fig. 4. First, the model estimates the probability if the bicycle is in motion (Rd1 or Rd2). The complementary probability represents the probability of Rd0. Then the probability of Rd1 and Rd2 are estimated as the outcome of the second stage.

The individual probabilities in the two-staged model are calculated by the following equations:

$$P_{Rd12}(v_{Bike}) = \frac{1}{1 + e^{-(\beta_{Rd12,0} + \beta_{Rd12,1} v_{Bike})}} \quad (7)$$

$$P_{Rd0}(v_{Bike}) = 1 - P_{Rd12}(v_{Bike}) \quad (8)$$

**Fig. 4.** Two stage architecture of the Rd-feature.

$$P_{Rd1}(v_{Bike}) = P_{Rd12}(v_{Bike}) * \left( 1 - \frac{1}{1 + e^{-(\beta_{Rd2,0} + \beta_{Rd2,1} v_{Bike})}} \right) \quad (9)$$

$$P_{Rd2}(v_{Bike}) = P_{Rd12}(v_{Bike}) * \frac{1}{1 + e^{-(\beta_{Rd2,0} + \beta_{Rd2,1} v_{Bike})}} \quad (10)$$

where  $P_{Rd,i}$  is the probability of each state of the Rd-feature and  $P_{Rd12}$  represents the combined probability estimate for the Rd1 and Rd2 states. The  $\beta_{Rd}$  coefficients are the trained parameters.  $v_{Bike}$  represents the independent input variable. Fig. 5 shows the results of the trained logit models. It is seen that the trained logit models show a typical threshold characteristic corresponding to the riding speed  $v_{Bike}$ .

### 2.5.2. Collision feature

The estimation of the collision feature requires a more complex structure. The input variables used here are the mass specific energy  $\Delta e_{xy,uc}$  and the bike orientation  $\gamma$ , since at the beginning of a collision the bicycle is supposed to be upright. Based on data analysis, the training data shows a correlation between the specific energy change and the current speed measurement during a collision. Therefore,  $v_{Bike}$  is also used as an input variable for detecting the collision feature.

It should be noted that a limitation of the logistic regression method is its linear combination of the gain vector  $\beta$  with the input variables  $\mathbf{X}$ . To prevent linear relationships, we apply a nonlinear transformation of the input variables and perform the model training in the non-linearly transformed feature space. Here, we use an exhaustive search method supported by domain knowledge to define the transformation rules. Fig. 6 shows the transformed input signals, where the tilde symbol denotes a transformed input variable.

In general, the staged architecture of the collision feature is similar to the presented architecture of the Rd feature (see Fig. 4). Therefore, similar to the probability estimation for the ride feature, the following equations are used for estimating the probability of the different collision levels (C1–C3, see Table 1):

$$P_{C123}([\tilde{v}_{Bike}, \tilde{\gamma}, \Delta e_{xy,uc}] = \mathbf{X}_C) = \frac{1}{1 + e^{-(\beta_{C,0} + \beta_{C,1} * \tilde{v}_{Bike} + \beta_{C,2} * \tilde{\gamma} + c_1 * \beta_{C,3} * \Delta e_{xy,uc})}} \quad (11)$$

$$P_{C0}(\mathbf{X}_C) = 1 - P_{C123}(\mathbf{X}_C) \quad (12)$$

$$P_{C1}(\mathbf{X}_C) = P_{C123}(\mathbf{X}_C) * \left( 1 - \frac{1}{1 + e^{-(\beta_{C,0} + \beta_{C,1} * \tilde{v}_{Bike} + \beta_{C,2} * \tilde{\gamma} + c_2 * \beta_{C,3} * \Delta e_{xy,uc})}} \right) \quad (13)$$

$$P_{C23}(\mathbf{X}_C) = P_{C123}(\mathbf{X}_C) * \frac{1}{1 + e^{-(\beta_{C,0} + \beta_{C,1} * \tilde{v}_{Bike} + \beta_{C,2} * \tilde{\gamma} + c_2 * \beta_{C,3} * \Delta e_{xy,uc})}} \quad (14)$$

$$\begin{aligned} P_{C2}(\mathbf{X}_C) = P_{C123}(\mathbf{X}_C) * P_{C23}(\mathbf{X}_C) * & \left( 1 - \frac{1}{1 + e^{-(\beta_{C,0} + \beta_{C,1} * \tilde{v}_{Bike} + \beta_{C,2} * \tilde{\gamma} + c_3 * \beta_{C,3} * \Delta e_{xy,uc})}} \right) \\ & - \frac{1}{1 + e^{-(\beta_{C,0} + \beta_{C,1} * \tilde{v}_{Bike} + \beta_{C,2} * \tilde{\gamma} + c_3 * \beta_{C,3} * \Delta e_{xy,uc})}} \end{aligned} \quad (15)$$

$$P_{C3}(\mathbf{X}_C) = P_{C123}(\mathbf{X}_C) * P_{C23}(\mathbf{X}_C) * \frac{1}{1 + e^{-(\beta_{C,0} + \beta_{C,1} * \tilde{v}_{Bike} + \beta_{C,2} * \tilde{\gamma} + c_3 * \beta_{C,3} * \Delta e_{xy,uc})}} \quad (16)$$

where  $c_1$  and  $c_3$  are scaling parameters of the energy input  $\Delta e_{xy,uc}$ . The model training is done for the medium C2-feature, which uses the unscaled energy. The introduction of the scaling parameters leads to equivalent coefficients of  $\beta_C$  (which are the trained hyperparameters) between the different model stages. If several collision levels are given as indices, the probability estimate is valid for at least one of these states. The analysis of the training data reveals that the detection of C1 events is only reasonable during standing phases (Rd0).

As a result, the collision feature based on the two transformed variables and the energy  $\Delta e_{xy,uc}$  is plotted in Fig. 7 for training the medium collision feature (C2, see Table 1). Transforming the input variables

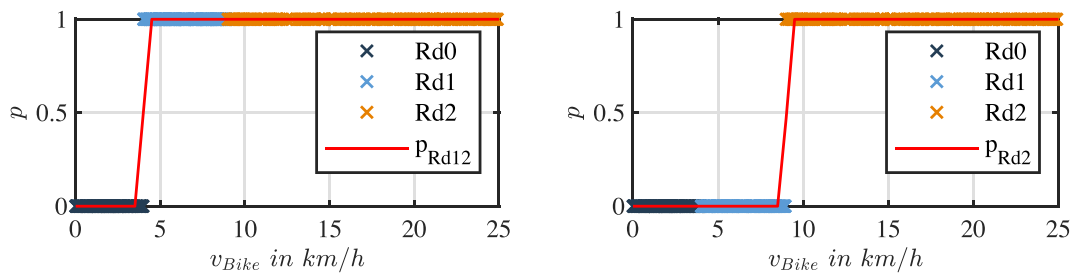


Fig. 5. Trained sigmoid functions for estimating the two staged Rd-feature.

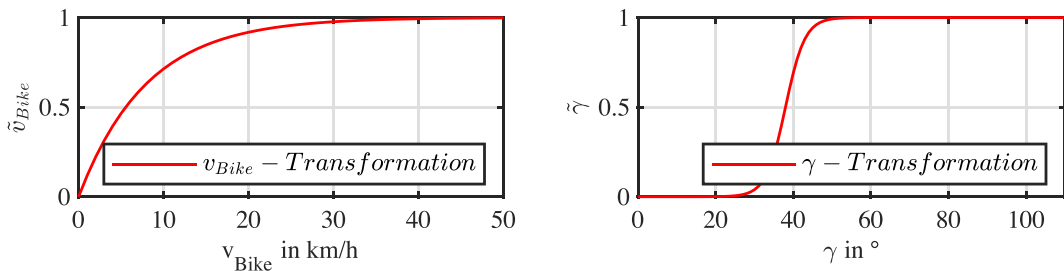
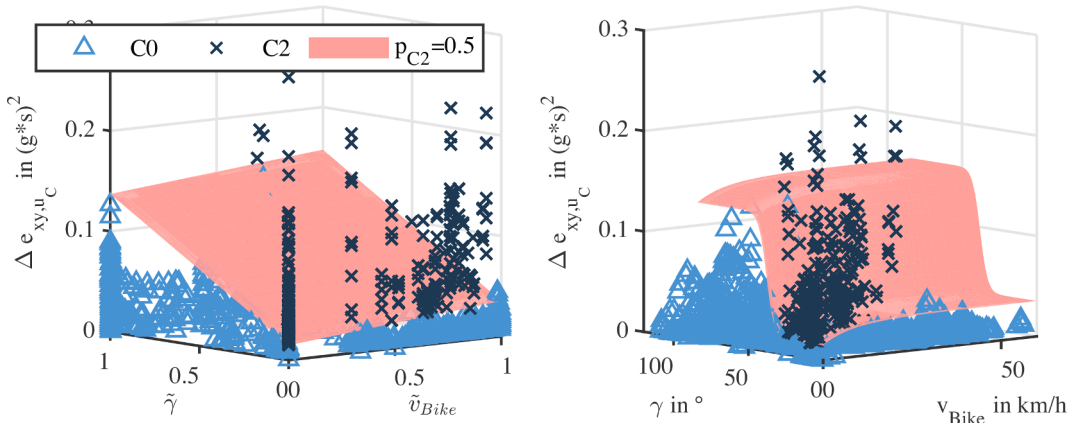
Fig. 6. Transformation models for speed  $v_{Bike}$  and bike orientation  $\gamma$ .

Fig. 7. Left: nonlinearly transformed feature space for medium collision classification, right: retransformed feature space for medium collision classification; hyperplanes visualize the trained model for a probability of 50% for a medium collision (C2).

according to the rules shown in Fig. 6, presents accurate classification results based on the linear 0.5-hyperplane in the transformed feature space. After this nonlinear transformation, the final model with a nonlinear relationship is obviously shown and the fitted nonlinear hyperplane enables highly precise classification results in the retransformed feature space.

The hyperplanes present the trained hyperparameter vector  $\beta_C$  at a probability threshold of 50%, which is trained as a logit model using the maximum likelihood method. The hyperplane is obtained by rearranging the model Eq. (15) after one freely chosen independent input variable. Then the remaining independent input variables are varied over the whole feature space and  $p_{C2}$  is set to 50% to generate the visualization of the characteristics of the classifier.

### 2.5.3. GroundHit feature

The independent input variables used for the GroundHit feature are the energy  $\Delta e_{xy,u_{GH}}$ , the fused bike orientation  $\gamma$  (since during a GroundHit the bicycle is supposed to be not upright) and the acceleration variance  $\sigma_{xy,u_{GH}}$ . The ANOVA results and the domain knowledge regarding the bicycle orientation during a GroundHit lead to this model

input selection.

Similarly, the logit model of the GroundHit feature also requires a nonlinear transformation of the input variables. The fused bike orientation  $\gamma$  is transformed according to the collision feature (see Fig. 6). The transformation of the variance  $\sigma_{xy,u_{GH}}$  is a sigmoid function similar to the  $\gamma$ -transformation.

Due to the fact that a binary decision between an actual GroundHit event (GH1) and a non-GroundHit situation (GH0) is needed, this model only has one stage. Therefore, the probabilities of the corresponding feature states are calculated as follows:

$$p_{GH1}(\tilde{\gamma}, \tilde{\sigma}_{xy,u_{GH}}, \Delta e_{xy,u_{GH}}) = \frac{1}{1 + e^{-(\beta_{GH,0} + \beta_{GH,1}\tilde{\gamma} + \beta_{GH,2}\tilde{\sigma}_{xy,u_{GH}} + \beta_{GH,3}\Delta e_{xy,u_{GH}})}} \quad (17)$$

$$p_{GH0}(\tilde{\gamma}, \tilde{\sigma}_{xy,u_{GH}}, \Delta e_{xy,u_{GH}}) = 1 - p_{GH1}(\tilde{\gamma}, \tilde{\sigma}_{xy,u_{GH}}, \Delta e_{xy,u_{GH}}) \quad (18)$$

where  $\beta_{GH}$  is the trained hyperparameter vector.

The two feature spaces for training the GroundHit feature are plotted in Fig. 8. It can be seen that the illustrated linear hyperplane ( $p_{GH} = 0.5$ ) in the transformed feature space exhibits clearly the trained model characteristics and that it shows a clear separation between the two

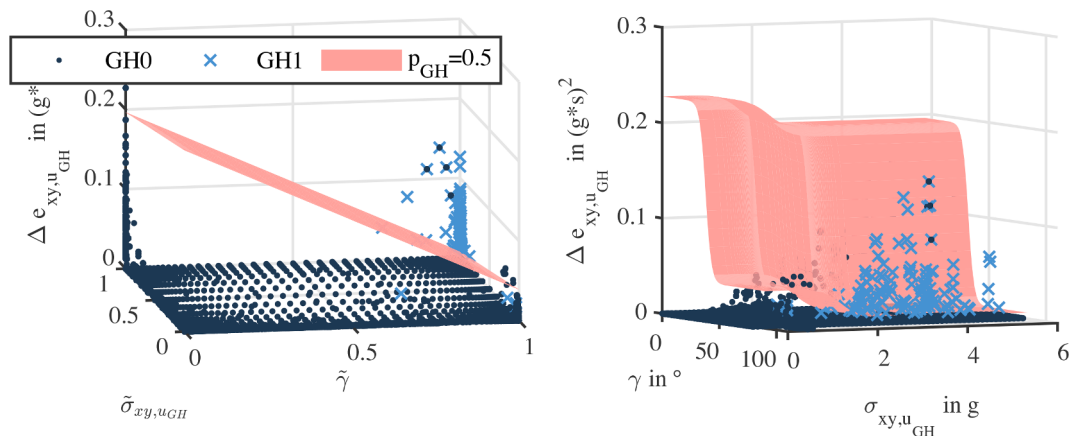


**Fig. 8.** left: nonlinearly transformed feature space for GroundHit classification, right: retransformed feature space for GroundHit classification; hyperplanes visualize the trained model for a probability of 50% for GroundHit (GH1).

populations.

#### 2.5.4. TipOver feature

This crash feature has a major influence on most real-world bicycle crashes, since during most accidents, the bicycle is going to tip or roll over and will be lying on one side afterwards. Due to the defined model states (see Table 1), two stages are used for the detection of this feature. The first stage analyzes the actual orientation of the bicycle. The second stage examines if a general TipOver (TO12) occurred, how this orientation change took place. This step enables the classification of so-called “NoseOver” (TO2) incidents when the bicycle system is rotating over the handlebar and the cyclist is falling in the same direction.

For the first stage, the pre-processed orientation signals  $\gamma$  and  $\gamma_{acc}$  are chosen as input variables. It is to note that  $\gamma$  responds fast due to the sensor fusion, while  $\gamma_{acc}$  shows a time delay due to the low-pass filtered acceleration signals. Both are necessary, e.g. for specific mountain bike scenarios with a short-term horizontal bicycle orientation (so-called “wall rides”).

Both variables require the same input transformation as the transformation of  $\gamma$  for the collision feature. Fig. 9 shows the non-linearly transformed and retransformed feature spaces for the first stage of the TipOver module.

The classification of TO2 events takes the current pitch angle of the bicycle into account. During NoseOver situations the roll angle is supposed to be smaller than the pitch angle and thus  $\psi$  is introduced. The low-pass filtered z-acceleration signal presents further meaningful classification characteristics. If the bike is upright, the z-axis is measuring the gravity. Caused by the time delay of the filter, this signal is able to proof that the bicycle has been upright just before an orientation change. Both  $\psi$  and  $\theta$  are transformed by further sigmoid functions.

The combination of both stages yields the following model equations, for estimating the probabilities of all three TipOver feature states:

$$p_{TO12}(\tilde{\gamma}, \tilde{\gamma}_{acc}) = \frac{1}{1 + e^{-(\beta_{TO12,0} + \beta_{TO12,1}\tilde{\gamma} + \beta_{TO12,2}\tilde{\gamma}_{acc})}} \quad (19)$$

$$p_{TO1}(\tilde{\gamma}, \tilde{\gamma}_{acc}) = 1 - p_{TO12}(\tilde{\gamma}, \tilde{\gamma}_{acc}) \quad (20)$$

$$p_{TO2}(\tilde{\theta}, \tilde{\psi}, \tilde{a}_{Bf,Lp,z}) = p_{TO12}(\tilde{\gamma}, \tilde{\gamma}_{acc}) * \frac{1}{1 + e^{-(\beta_{TO2,0} + \beta_{TO2,1}\tilde{\theta} + \beta_{TO2,2}\tilde{\psi} + \beta_{TO2,3})}} \quad (21)$$

$$p_{TO2}(\tilde{\theta}, \tilde{\psi}, \tilde{a}_{Bf,Lp,z}) = p_{TO12}(\tilde{\gamma}, \tilde{\gamma}_{acc}) * \frac{1}{1 + e^{-(\beta_{TO2,0} + \beta_{TO2,1}\tilde{\theta} + \beta_{TO2,2}\tilde{\psi} + \beta_{TO2,3})}} \quad (22)$$

Fig. 10 shows the non-linear-transformed and retransformed feature spaces for the second stage of the TipOver model. It can be clearly seen that the  $p_{TO2} = 0.5$  hyperplanes in both feature spaces confirm the successful training. In addition, this exploits the benefit of the nonlinear transformation of the independent input variables.

### 3. Data acquisition

Due to the availability of power supply and sensor equipment, EPACs are extremely suitable for data acquisition and system integration. Therefore, this work is based on the data accumulated by EPACs. Nevertheless, due to similar vehicle geometries (MacArthur and Kobel, 2014) and similar average speeds (classic bicycles: 15.3 km h<sup>-1</sup>, EPACs: 17.4 km h<sup>-1</sup>, Schleinitz et al., 2017) it is expected that the methods and

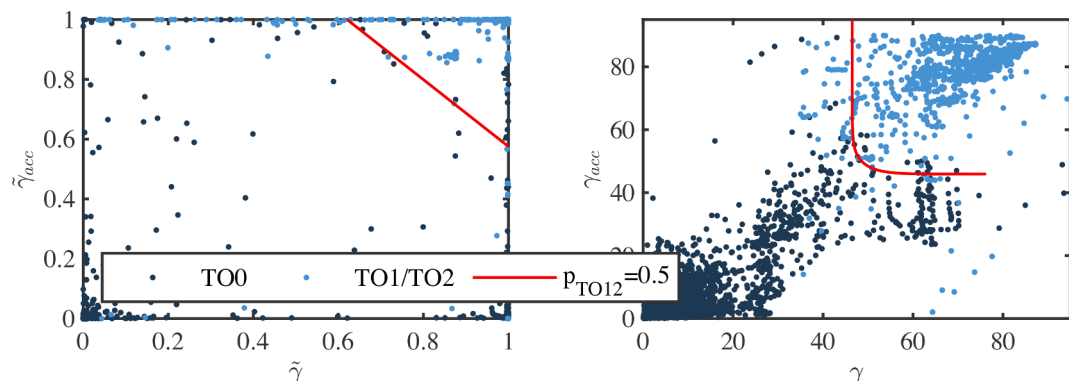


**Fig. 9.** Left: non-linearly transformed feature space for the first stage of the TipOver feature, right: retransformed feature space for the first stage of the TipOver feature; red separation lines show the trained model for a probability of 0.5 for TO12.

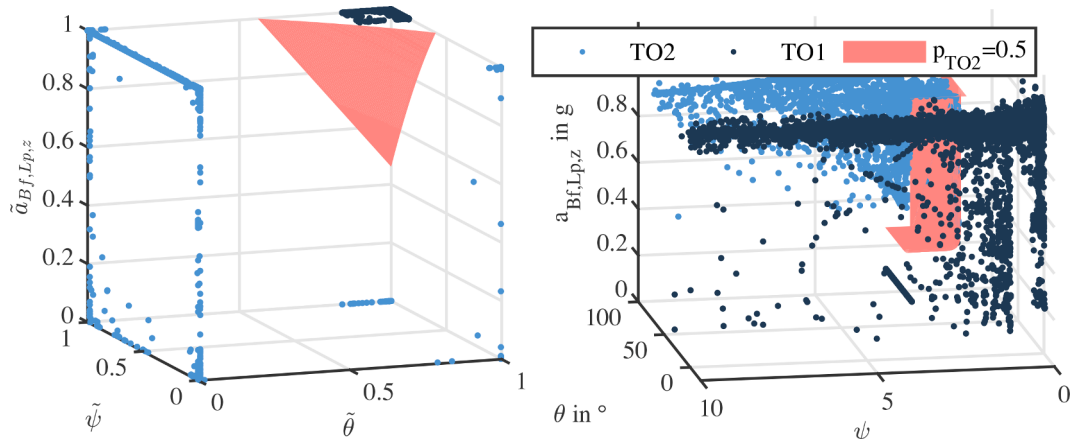


**Fig. 10.** Left: transformed feature space for the second stage of the TipOver feature, right: retransformed feature space for the second stage of the TipOver feature; hyperplanes show the trained model for a probability of 50% for TO2.

results presented in this paper will also show potential for classic bicycles. We use the 6DOF-IMU-data collected from the sensors with a rigid link to the bicycle. The IMUs are standard consumer-grade sensors with measurement ranges up to 16 g and  $2000^{\circ}\text{s}^{-1}$ . Direct speed measurement is also used to enhance the classification results.

The database used in this study for the model training and validation consists of three parts. The first part is a naturalistic driving study with 60 bicyclists (85% male, 15% female, mean age 34 years at study start, min. age: 22 years and max. age: 55 years) over two years. During that period, 20 real crashes occurred. In addition, this part includes data from 20,000 km ridden distance of daily cycling. Furthermore, various scenarios like sportive and mountain bike situations as well as varying environmental circumstances (during all four seasons and weather conditions) are covered.

The second part is a dataset with 183 crash tests. These tests were performed on a test track with a crash dummy and a crash car (see Fig. 11). The aim of this crash study is to mimic common bicycle accidents and to test a variety of different crash scenarios.

The third part contains a dataset from corner case tests with mountain bikes (e.g. jumps, drops, wall rides, stair set rides and single trails), which were performed by a professional bicyclist (Schlie, 2019). Fig. 11 provides an insight into these tests. Further tests regarding the bike handling, e.g. stopping and laying the bike to one side, were also performed to enhance the corner case subset. Table 3 provides an overview of the three subsets and their key facts of the data used in this study.

**Table 3**

Overview of the data-base for model training and validation.

#	Name	Description	num. crashes	Ridden km
1	MRDC	multi-rider-data-collection, naturalistic driving data, 60 test persons	20	20,000
2	CT	crash test series	183	5
3	CCT	corner case tests	1	470

All IMU signals were logged with a sample frequency  $f_s = 100\text{ Hz}$ . The different IMU sensors used belong to the category of consumer hardware.

An independent model validation requires the data to be split into training and validation data. Therefore, one third of the CT-subset is used for data analysis and training. Two thirds are reserved for model validation. Approximately 99% of the MRDC subset and 90% of the CCT data are used for validation. The retaining MRDC data (<1%, mountain bike cases) and corner cases (10%) are employed for the training.

#### 4. Results and discussion

In this section, an experimental validation of the overall probabilistic model is performed based on the selected validation data (see Section 3).

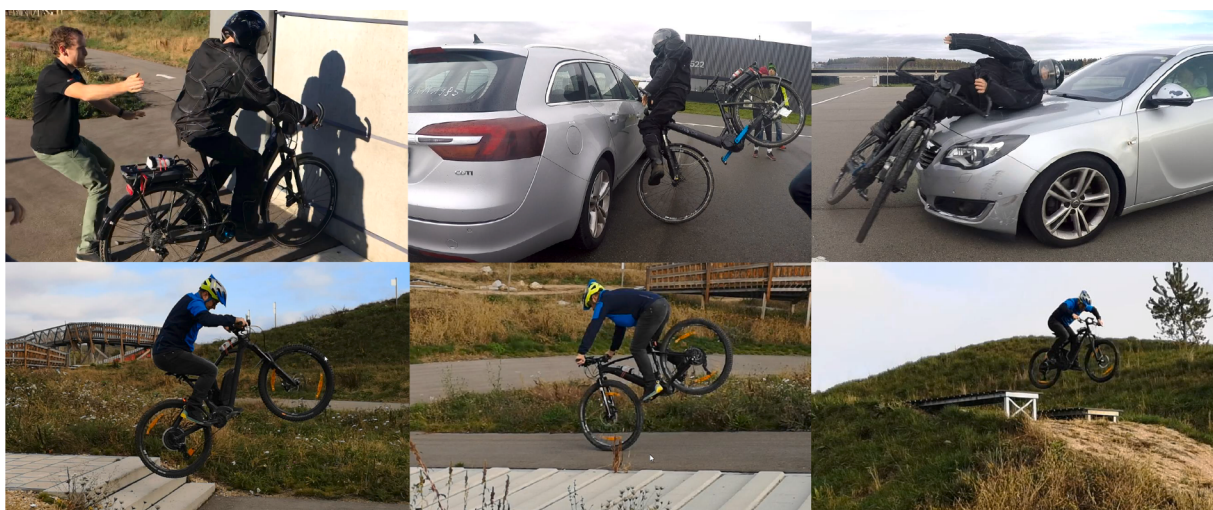


**Fig. 11.** Photographic documentation of data-acquisition; above: crash test series; below: corner case tests.

The time-dependent data profiles are divided in segments of equal lengths in order to test the model on standard driving distances, which leads to approximately 3400 datasets. The validation of the approach is implemented in MATLAB.

#### 4.1. Experimental validation of the binary crash detection

The final model outputs of the approach are evaluated according to the overall crash probability  $p_c$  and the crash class with the maximum probability. First, we analyze our approach regarding the general crash detection by evaluating the relative amount of true-positive (TP), true-negative (TN), false-positive (FP) and false-negative (FN) (Saito and Rehmsmeier, 2015) and at different threshold levels of the crash probability  $p_c$  (see Fig. 12).

As shown in Fig. 12, if the threshold is given, for example, at a level of 50%, it leads to a TN-ratio of 99.6% and a TP-ratio (sensitivity) of 96.8%. The model accuracy  $\frac{TP+TN}{numdatasets}$  at this operating point is at 99.5%. The highly unbalanced dataset causes this shift of the model accuracy towards the TN-rate. The validation dataset only shows a small amount of crash cases compared to the non-crash cases, due to the extensive crash data acquisition.

To evaluate the binary (i.e., crash or non-crash) model, we use the receiver operating characteristics (ROC) and precision recall (PRC) plots (Saito and Rehmsmeier, 2015). The ROC analysis sets the TP-ratio and FP-ratio in a direct relation and compares it with a general random process (baseline) (Hanley and Mcneil, 1982). Due to the unbalance of the validation dataset, i.e. significantly more negative than positive cases, a PRC analysis needs to be performed (Saito and Rehmsmeier, 2015), since the PRC curve includes the unbalance in the precision ratio and the baseline. The resulting plots are shown in Fig. 13.

In Fig. 13, the ROC-AUC (area under the curve) value describes the classification accuracy of the final model. The two curves represent possible operating points of the classifier. As shown in Fig. 13, two operating points are illustrated. The red circle exhibits a precision of 98.3%, a FP-ratio of 0.06% and a TP-ratio 92.8%. This operating point is the result of a crash probability threshold of 97.7%.

To improve the TP-ratio, the crash probability threshold is set to 50.1% at the second operating point (marked as a red cross). Here, the result shows a precision of 90.3%, a FP-ratio of 0.4%, a TP-ratio 96.8% (sensitivity) and a specificity of 99.6%. This selection of the second

operating point emphasizes the importance of the cyclists' safety. An analysis of the remaining FN-cases exhibits that these cases show a low accident degree and low accident severity, and thus the rider should not be injured severely. This operating point would lead to one false-positive every 86 h respectively 1500 km of cycling based on our validation dataset and the mean speed of EPAC riders of 17.4 km h<sup>-1</sup> (Schleinitz et al., 2017). However, if the user is able to abort the automatically detected accident (FP events) with the help of a defined user interface, most false-positives will be rejected and no expenditure will be generated on the side of the responsible PSAP (public safety answering point).

As a result, ROC and PRC can be used to evaluate the final model and threshold levels for the binary crash detection. The most important requirement here is to detect as many accidents as possible in terms of the safety of the cyclist. Furthermore, it is required that the amount of FPs be at a low level, in order to reduce the number of false alerts to rescue services.

The validation results shown above confirm that the trained classifier shows high potential of our approach for bicycle crash detection, especially in terms of an automatic emergency service.

#### 4.2. Experimental validation of the crash classification

To validate the crash classification, we separate the evaluation of the estimated crash classes into two parts, i.e. the super-crash class and the sub-crash class.

For this purpose, we check the crash class with the highest probability estimate (see Eq. (6)) in each dataset and evaluate only the crash datasets. Fig. 14 shows the resulting TP-ratios of the super-crash class and the sub-crash class, respectively.

It is shown in Fig. 14 that the TP-ratio for the super-crash class is 92.56% and thus it confirms the validity of the trained classifier, while the validation of the sub-crash classification reveals a TP-ratio of 69.42%. The reasons for this relatively lower value is because of some missing objects and measurable definitions regarding the sub-crash class labeling of the ground truth during the data acquisition. Nevertheless, the presumed misclassifications often showed reasonable sub-crash classes. After the testing, a manual analysis approved these cases, too. However, a reduced sub-crash class TP-ratio compared to the super class TP-ratio is expected, because classifying into more detailed categories is highly challenging.

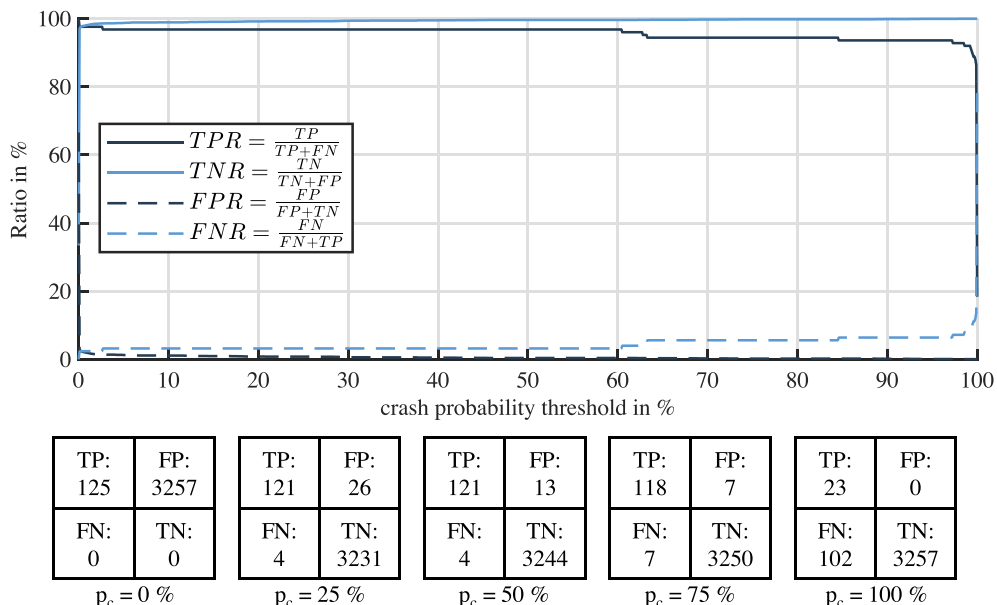


**Fig. 12.** Validation results regarding general crash detection, evaluated at various threshold levels of the crash probability  $p_c$ , based on test data; top: relative results as ratios, bottom: absolute results, one sample corresponds to one normalized test ride.

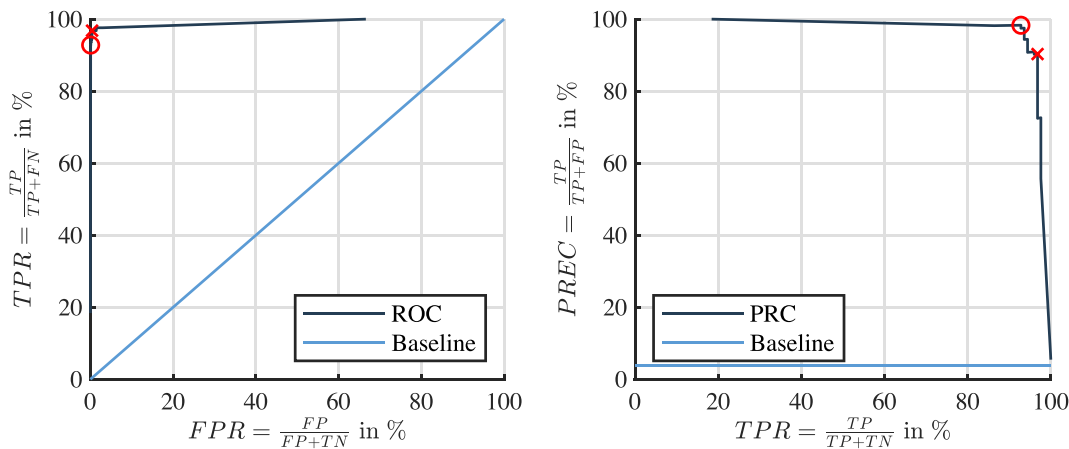


**Fig. 13.** Left: ROC analysis, baseline represents a random process, ROC-AUC is 0.9871; right: PRC analysis, baseline represents the ratio of the dataset-balance, PRC-AUC is 0.9692; red marks are two exemplary operating points.

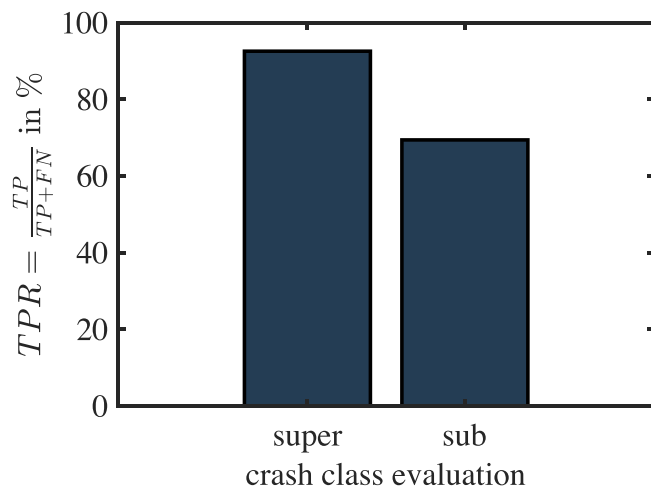


**Fig. 14.** Analysis of the crash classification results regarding super- and sub-crash classes, only crash datasets are considered.

In summary, the experimental test and validation show satisfactory classification results in terms of the super-crash class estimation. Therefore, our approach is able to provide further plausible crash information to an automatic emergency system and meanwhile it enables an automatic data acquisition for a bicycle accident database.

The sub-crash class validation results also exhibit a relatively high number of correct classifications, considering the unclear labeling of the ground truth sub-crash classes in the validation data. However, further analysis of the sub-crash classes should be performed in order to define measurable conditions during future data acquisition.

Besides the Matlab implementation, we translated the model into C and implemented it on an Atmel SAM3X8E microcontroller (ARM-Cortex-M3) for analyzing the embedded real-time requirements. As a result, the probabilistic model was realized with an execution rate of 100 Hz.

## 5. Conclusions

In this paper, we proposed a bicycle crash classification approach using logit models with transformed input signals for generating probability estimates of defined bicycle crash features. These crash features allow the categorization of typical cycling events and accident scenarios with varying kinematic trajectories.

For model training and validation, we established an extensive database by performing a naturalistic driving study and a series of

bicycle crash tests. The data were collected from an IMU sensor on electric bicycles. Beside the studied case, the proposed approach shows a potential to be applied for crash classification of classic bicycles due to similar riding and accident dynamics.

The validation results indicate the usefulness of the proposed approach. The accuracy of the presented method for the binary crash detection is high (FP-ratio = 0.4%; TP-ratio = 96.8%), which is essential for a reliable automatic emergency service system and an automatic crash data acquisition. The validation of the classification into super- and sub-crash classes also showed satisfactory results.

Future work will focus on applying the approach on as many bicycles as possible to perform large-scale automatic data acquisition. In addition, specific definitions can be introduced for the ground truth of the sub-class labeling. Moreover, based on such automatically accumulated high amount of data, an extension of the model with further machine learning methods is possible.

## CRediT authorship contribution statement

**Jan Schnee:** . **Jürgen Stegmaier:** . **Pu Li:** Supervision, Methodology, Writing – original draft, Writing – review & editing.

## Declaration of interest

Schnee and Stegmaier are both working for Robert Bosch GmbH in the Department of eBike Systems.

## Acknowledgements

The authors gratefully acknowledge the support of Bosch eBike Systems especially during the extensive data acquisition.

## References

- Algamal, Z.Y., Lee, M.H., 2015. Penalized logistic regression with the adaptive lasso for gene selection in high-dimensional cancer classification. *Expert Syst. Appl.* 42 (23), 9326–9332.
- Bonyr, A., Gczy, A., Krammer, O., Sntha, H., Ills, B., Kmn, J., Szalay, Z., Hank, P., Harsnyi, G., 2017. A review on current ecall systems for autonomous car accident detection. In: 2017 40th International Spring Seminar on Electronics Technology (ISSE), pp. 1–8.
- Bundesamt fuer Strassenwesen, 2016. Verkehrssicherheit von radfahrern analyse sicherheitsrelevanter motive, einstellungen und verhaltensweisen, Internet (Aug 2016). URL: [https://www.bast.de/BAST\\_2017/DE/Publikationen/Foko/Downloads/2017-2010/2016-08.pdf?blob=publicationFile&v=4](https://www.bast.de/BAST_2017/DE/Publikationen/Foko/Downloads/2017-2010/2016-08.pdf?blob=publicationFile&v=4).
- Bosch eBike, Internet 2018. URL: <https://www.bosch-ebike.com/de/produkte/abs/>.
- Candefjord, S., Sandsj, L., Andersson, R., Carlborg, N., Szakal, A., Westlund, J., Sjqvist, B., 2014. Using smartphones to monitor cycling and automatically detect accidents - towards ecall functionality for cyclists, in: Proceedings, International Cycling Safety Conference 2014, 2014.

- Chavis, C., Lee, Y.-J., Dadvar, S. 2018. Analysis of bicycle and pedestrian crash causes and interventions.
- Chen, C.-K., Chu, T.-D., Zhang, X.-D., 2019. Modeling and control of an active stabilizing assistant system for a bicycle. Sensors 19, 248. <https://doi.org/10.3390/s19020248>.
- Dalgaard, P., 2008. *Introductory Statistics with R*, 2nd Edition. Springer.
- DiGioia, J., Watkins, K.E., Xu, Y., Rodgers, M., Guensler, R., 2017. Safety impacts of bicycle infrastructure: A critical review. J. Saf. Res. 61, 105–119. <https://doi.org/10.1016/j.jsr.2017.02.015>. URL: <http://www.sciencedirect.com/science/article/pii/S0022437517301524>.
- Figo, D., Diniz, P.C., Ferreira, D.R., Cardoso, J.M., 2010. Preprocessing techniques for context recognition from accelerometer data. Pers. Ubiquit. Comput. 14 (7), 645–662.
- Garmin, Garmin incident detection, Internet. URL:<https://www8.garmin.com/manuals/webhelp/edge520/EN-US/GUID-F109FB24-B55D-49D2-B388-D042E7FBA965.html>.
- Gelmini, S., Strada, S., Tanelli, S., Savaresi, M., Tommasi, C.D. 2019. Automatic crash detection system for two-wheeled vehicles: design and experimental validation, IFAC-PapersOnLine 52(5):498–503, 9th IFAC Symposium on Advances in Automotive Control AAC 2019. doi: 10.1016/j.ifacol.2019.09.079. URL:<http://www.sciencedirect.com/science/article/pii/S2405896319307025>.
- Gu, W., Zhou, Z., Zhou, Y., Zou, H., Liu, Y., Spanos, C.J., Zhang, L., 2017. Bikemate: Bike riding behavior monitoring with smartphones. In: Proceedings of the 14th EAI International Conference on Mobile and Ubiquitous Systems: Computing, Networking and Services, pp. 313–322.
- Hagemeister, C., Bunte, H., Brammer, N., Wagner, P. 2015. Unfile Iterer radfahrender dunkelziffer, unfallunstnde und risikoverhalten, in: 1. Kongress der Fachgruppe Verkehrspychologie.
- Hanley, J., Mcneil, B., 1982. The meaning and use of the area under a receiver operating characteristic (roc) curve. Radiology 143, 29–36. <https://doi.org/10.1148/radiology.143.1.7063747>.
- Hastie, T., Tibshirani, R., Friedman, J., 2001. *The Elements of Statistical Learning, Springer Series in Statistics*, Springer. New York Inc., New York, NY, USA.
- Iso 8855:2011, 2011. road vehicles – vehicle dynamics and road-holding ability – vocabulary.
- Juhra, C., Wieskter, B., Chu, K., Trost, L., Weiss, U., Messerschmidt, M., Malczyk, A., Heckwolf, M., Raschke, M., 2012. Bicycle accidents do we only see the tip of the iceberg?: A prospective multi-centre study in a large german city combining medical and police data. Injury 43 (12), 2026–2034. <https://doi.org/10.1016/j.injury.2011.10.016>. URL: <http://www.sciencedirect.com/science/article/pii/S0020138311005110>.
- MacArthur, J., Kobel, N. 2014. Regulations of e-bikes in north america.
- Madgwick, S., 2010. An efficient orientation filter for inertial and inertial/magnetic sensor arrays. Report x-io and University of Bristol (UK) 25, 113–118.
- Maier, O., Pfeiffer, M., Wehner, C., Wrede, J. 2015. Empirical survey on bicycle accidents to estimate the potential benefits of braking dynamics assistance systems, in: 4th Int. Cycling Safety Conf., Hannover, Germany, 2015.
- Olivier, J., Creighton, P., 2016. Bicycle injuries and helmet use: a systematic review and meta-analysis. Int. J. Epidemiol. 46 (1), 278–292. <https://doi.org/10.1093/ije/dyw153> arXiv: <https://academic.oup.com/ije/article-pdf/46/1/278/13733257/dyw153.pdf>.
- Ortlepp, P., Jrg und Butterwegge, Unfalltypen katalog leitfaden zur bestimmung des unfalltyps.
- Parviainen, J., Collier, J., Pihlstrm, T., Takala, J., Hanski, K., Lumiaho, A., 2014. Automatic crash detection for motor cycles. In: IECON 2014–40th Annual Conference of the IEEE Industrial Electronics Society, pp. 3409–3413. <https://doi.org/10.1109/IECON.2014.7049003>.
- Pucher, J., Buehler, R. 2016. Safer cycling through improved infrastructure.
- Rajamani, R., Jeon, W., et al., 2018. A novel collision avoidance system for a bicycle. Tech. rep., Roadway Safety Institute.
- Roberson, B. 2020. Forbes: Bike sales get a big boost in perfect storm of demand, covid-19 recovery and ebike maturity, Internet (May 2020). URL: <https://www.forbes.com/sites/billroberson/2020/05/29/bike-sales-get-a-big-boost-in-perfect-storm-of-demand-covid-19-recovery-and-ebike-maturity/>.
- Roelleke, M., Jauch, T., Koehler, A. 2001. Rückhaltesystem mit einer rückhalteeinrichtung zum schutz wenigstens eines passagiers [restraint system for the protection of at least a single passenger], dE Patent 10,042,376. URL: <https://encrypted.google.com/patents/DE10042376C1?cl=nl>.
- Sabatini, A.M., 2006. Quaternion-based extended kalman filter for determining orientation by inertial and magnetic sensing. IEEE Trans. Biomed. Eng. 53 (7), 1346–1356.
- Saito, T., Rehmsmeier, M., 2015. The precision-recall plot is more informative than the roc plot when evaluating binary classifiers on imbalanced datasets. PLoS One 10 (3), 1–21. <https://doi.org/10.1371/journal.pone.0118432>.
- Schepers, J., Fishman, E., [den Hertog], P., Wolt, K.K., Schwab, A. 2014. The safety of electrically assisted bicycles compared to classic bicycles, Accident Anal. Prevent. 73:174–180. doi:10.1016/j.aap.2014.09.010. URL:<http://www.sciencedirect.com/science/article/pii/S0001457514002668>.
- Schleinitz, K., Petzoldt, T., Franke-Bartholdt, L., Krems, J., Gehlert, T., 2017. The german naturalistic cycling study—comparing cycling speed of riders of different e-bikes and conventional bicycles. Saf. Sci. 92, 290–297.
- Schlie, S. 2019. Professional mtb-rider. URL: <http://bikeschlie.de/>.
- Schnee, J., Stegmaier, J., Lipowsky, T., Li, P., 2020. Auto-correction of 3d-orientation of imus on electric bicycles. Sensors 20 (3), 589. <https://doi.org/10.3390/s20030589>.
- Scholz, F.W., Stephens, M.A., 1987. K-sample anderson-darling tests. J. Am. Stat. Assoc. 82 (399), 918–924.
- Smaldone, S., Tonde, C., Ananthanarayanan, V., Elgammal, A., Iftode, L. 2010. Improving bicycle safety through automated real-time vehicle detection.
- Specialized, This helmet calls for help, Internet. URL: <https://www.specialized.com/us/en/stories/angi>.
- Statista, Absatz von e-bikes in deutschland von 2009 bis 2018 [epac sales in germany from 2009 to 2018], Internet (Mar. 2019). URL: <https://de.statista.com/statistik/daten/studie/152721/umfrage/absatz-von-e-bikes-in-deutschland/>.
- Statistisches Bundesamt, Verkehr-Verkehrsunfälle, Fachserie 8, Reihe 7, Statistisches Bundesamt (Destatis), 2020.
- Statistisches Bundesamt, Verkehrsunfälle - kraftrad- und fahrradunfälle im strassenverkehr 2019, [bicycle accident statistics in road transport in germany 2019], Internet (2020). URL: <https://www.destatis.de/DE/Themen/Gesellschaft-Umwelt/Verkehrsunfaelle/Publikationen/Downloads-Verkehrsunfaelle/unfaelle-zweirad-5462408197004.pdf>.
- Tabei, F., Askarian, B., Chong, J.W., 2021. Accident detection system for bicycle riders. IEEE Sens. J. 21 (2), 878–885. <https://doi.org/10.1109/JSEN.2020.3021652>.
- Tocsen, Tocsen calls if you crash, Internet. URL: <https://www.tocsen.com/de>.
- Usami, Y., Ishikawa, K., Takayama, T., Yanagisawa, M., Togawa, N., 2018. Bicycle behavior recognition using sensors equipped with smartphone. In: 2018 IEEE 8th International Conference on Consumer Electronics-Berlin (ICCE-Berlin) IEEE, pp. 1–6.
- Wu, Yuanxin, Hu, Xiaoping, Hu, Dewen, Li, Tao, Lian, Junxiang, 2005. Strapdown inertial navigation system algorithms based on dual quaternions. IEEE Trans. Aerosp. Electron. Syst. 41 (1), 110–132. <https://doi.org/10.1109/TAES.2005.1413751>.
- Zhang, Z., Jiang, Y., 2017. Analysis of 217 death of road traffic accident case about electric bicycle. Chin. J. Foren. Med. 32 (z1), 1–3.